

Magneto-Conductance Anisotropy and Interference Effects in Variable Range Hopping

Ernesto Medina

Intevep SA, Apartado 76343, Caracas 1070A, Venezuela

Mehran Kardar

Department of Physics, Massachusetts Institute of Technology, Cambridge, MA 02139, U.S.A.

Rafael Rangel

Departamento de Física, Universidad Simón Bolívar, Apartado 89000, Caracas 1080A, Venezuela

(August 16, 2018)

Abstract

We investigate the magneto-conductance (MC) anisotropy in the variable range hopping regime, caused by quantum interference effects in three dimensions. When no spin-orbit scattering is included, there is an increase in the localization length (as in two dimensions), producing a large positive MC. By contrast, with spin-orbit scattering present, there is no change in the localization length, and only a small increase in the overall tunneling amplitude. The numerical data for small magnetic fields B , and hopping lengths t , can be collapsed by using scaling variables $B_{\perp}t^{3/2}$, and $B_{\parallel}t$ in the perpendicular and parallel field orientations respectively. This is in agreement with the flux through a ‘cigar’-shaped region with a diffusive transverse dimension proportional to \sqrt{t} . If a single hop dominates the conductivity of the sample, this leads to a characteristic orientational ‘finger print’ for the MC anisotropy. However, we estimate that many hops contribute to conductivity of typical

samples, and thus averaging over critical hop orientations renders the bulk sample isotropic, as seen experimentally. Anisotropy appears for thin films, when the length of the hop is comparable to the thickness. The hops are then restricted to align with the sample plane, leading to different MC behaviors parallel and perpendicular to it, even after averaging over many hops. We predict the variations of such anisotropy with both the hop size and the magnetic field strength. An orientational bias produced by strong electric fields will also lead to MC anisotropy.

71.55.Jv, 05.40.+j, 72.20.Dp, 75.10.Nr

I. INTRODUCTION

Striking quantum interference (QI) effects have been observed in experiments on *insulating* materials [1–4]. These observations are of particular interest, as they point to quantum coherence phenomena for strongly localized electrons, where naively they may not have been expected to occur over length scales appreciably larger than the localization length ξ . A theoretical explanation was first proposed by Nguyen, Spivak and Shklovskii (NSS) [5] in the context of Mott Variable Range Hopping (VRH) [6]: Phase coherence is maintained over the long distances between phonon assisted tunneling events, which grow with decreasing temperature T as $\exp(T_0/T)^{1/(D+1)}$ in D spatial dimensions. The resulting coherence length can be quite large (typically of the order of $20 - 50\xi$). In this work, we consider the three dimensional NSS model and focus on the dependences of the conductance and its fluctuations on the relative orientations of the magnetic field and the dominant hop.

The initial indications of QI came from observations of a strong positive magneto-conductance (MC) in materials that exhibit VRH behavior [7]. In a single impurity picture, the action of the magnetic field is to further confine electrons already localized around the impurity. This would result in a negative MC which is not the case in experiments for weak magnetic fields. Further evidence is provided by the orbital nature of the MC [2] observed in *InO* films of varying thickness. While experiments show an isotropic MC for thick samples, anisotropy sets in when the film thickness is close to the Mott hopping length. Such anisotropy precludes explanations in terms of scattering of electron spin by magnetic impurities [8], which are necessarily isotropic with respect to the field direction, pointing instead to interference effects due to the electron orbits. Finally, in a careful set of experiments, Orlov et al [1] and Milliken and Ovadyahu [3] demonstrate the presence of reproducible conductance fluctuations or magneto-fingerprints, generally regarded as a clear signature of QI effects.

The NSS model considers the QI between the many virtual paths that the electron can take while tunneling under the barrier between two distant impurity centers. In the tunnel-

ing process, the hopping electrons with energies near the Fermi level, encounter impurities with energies outside the Mott energy strip. These impurities are considered as the source of elastic scattering events under the barrier. Since the contribution of each virtual path (tunneling through a barrier) is exponentially damped by the distance it covers, it is sufficient to ignore back-scattering and focus on the (directed) paths that only undergo forward scattering between the initial and final impurities.

The initial numerical studies of the NSS model (on relatively small systems) [5] indeed confirmed that it yields the correct sign for the MC. Subsequently, Sivan, Entin-Wohlman, and Imry [9] provided a theoretical analysis that agrees with much of the early NSS results. The critical hop is identified from the condition of producing a percolating network of random resistors [10], while the probability distribution for individual hops is calculated by assuming that the contributing virtual paths are uncorrelated. The latter assumption, which we shall refer to as the Independent Path Approximation (IPA), was shown to be invalid by Shapir and Wang [12], since, in low dimensions, the paths must intersect at some scattering sites. Eventually, the correct form of the hopping probability distribution was calculated by Medina et al [13], by incorporating the correlations between the virtual paths. The analytical results, confirmed by extensive numerical simulations on very large sizes, indicate that the positive MC in this model actually corresponds to an increase in the localization length with the magnetic field in the absence of Spin-Orbit scattering. This prediction is supported, at least qualitatively, by recent experiments on *InO* [2] and *YSi* [14]. While the IPA scheme cannot produce a change in the localization length, an alternative approach to strong localization, based on Random Matrix Theory (RMT) [14], also produces such an effect. The latter, which is exact only for quasi-one dimensional systems, predicts a doubling of the localization length.

There are conflicting theoretical and experimental observations in the presence of Spin-Orbit scattering. The first experimental study on *InO* [15] showed MC behavior resembling that of the weak localization regime; i.e. a positive MC for low fields, changing to negative at higher fields. On the other hand, more recent experiments [14] on *YSi* show negative

MC for all applied fields. On the theoretical side, both the IPA scheme [16], and the correct accounting of correlations [17], yield a positive MC without changes in the localization length. (In fact the IPA results for MC are exact in the presence of strong SO.) Finally, the Random Matrix [14] approach finds a negative MC caused by a universal decrease of the localization length by a factor of two. These issues are discussed in greater detail in reference [19], and will not be discussed further in the present work.

In this work we study the NSS model in three dimensions, with and without spin-orbit scattering. An important new feature is that we must now take into account the relative directions of the magnetic field and the dominant hop. This issue is most relevant experimentally for samples that are small enough (or at such low temperatures) to include only a single dominant hop. By measuring the MC anisotropy as a function of the direction of the magnetic field, it is possible to locate the orientation of this dominant hop! Field dependences parallel and perpendicular to this orientation can then be used to further test the current models of coherence in the localized regime. There is, however, a certain amount of internal averaging when the conductance is dominated by several hops. Some insight about the nature of the hops can then be obtained by examining the MC anisotropy of thin films, as a function of their thickness and orientation to the magnetic field.

II. THE NSS MODEL

Low temperature conduction in the strongly localized regime is dominated by thermal hopping. At the lowest temperatures localized electrons lack enough thermal energy to hop to neighboring sites. On the other hand, electrons cannot wander too far away from their localization point due to the exponential decay of the wave function. The balance of these competing tendencies results in an optimal hopping length and leads to Mott's law for VRH [6]. Each of these hops may be represented by an effective resistor (hopping probability) in a network which can then be solved for the macroscopic conductance of the sample. The picture of the Miller-Abrahams (MA) [20] network is central to the understanding

of hopping conduction. The effective resistance of the MA network was first estimated by Ambegaokar, Halperin, and Langer (AHL) [10], and Shklovskii and Efros [11], using a percolation argument: Due to the exponentially large values of the resistors in the network, the macroscopic conductance is dominated by a single bottle-neck resistor on a percolating network. (We shall later discuss the modifications due to multiple hops). This simple argument provides a powerful tool, since it is then sufficient to determine the variations of a single hop with various external (applied fields) or internal (doping, correlation effects, anisotropy) physical parameters [21].

The model proposed by NSS examines QI effects for the dominating hop. Due to the long distance of the hop, typically $R \sim \xi(T_0/T)^{1/(D+1)} \sim 20 - 50\xi$, electrons scatter off many impurities on route to the final site. While at the end of the process there is some loss of phase coherence (due to inelastic scattering by phonons), the intermediate scattering is elastic. To study QI processes for the hop, the NSS model places the impurities on the sites of a regular lattice; e.g. the cubic lattice in Fig. 1. The interference effects are maximized if the initial and final sites for the hop are chosen at diagonally opposite end-points. Electrons can then follow many different virtual paths from the initial to the final site. The overall tunneling amplitude is computed by summing all (virtual) paths between the two points, each contributing an appropriate quantum mechanical complex weight. These weights are obtained from an Anderson tight-binding Hamiltonian

$$\mathcal{H} = \sum_i \epsilon_i a_i^\dagger a_i + \sum_{\langle ij \rangle} V_{ij} a_i^\dagger a_j, \quad (1)$$

where ϵ_i are the impurity site energies, and V_{ij} represent the nearest neighbor couplings or transfer terms. NSS further simplify the problem by choosing site energies distributed according to

$$\epsilon_i = \begin{cases} +W & \text{with probability } p, \\ -W & \text{with probability } (1 - p), \end{cases}$$

and a transfer term

$$V_{ij} = \begin{cases} V & \text{if } i, j \text{ are nearest neighbors,} \\ 0 & \text{otherwise.} \end{cases}$$

We shall henceforth set $p = 1/2$. To describe strong localization, the Anderson parameter is taken to be much smaller than one ($V/W \ll 1$). This corresponds physically to a strongly disordered sample where the width of the bands ($\sim 2V$) centered at energies $\pm W$ is much smaller than their energy difference to the Fermi level.

The effective hopping matrix element can be computed using a locator expansion [18] [19]. The overlap amplitude (Green's function) between the initial and final sites is given by

$$\langle \Phi | G(E) | \Psi^+ \rangle = \sum_{\Gamma} \prod_{i_{\Gamma}} \frac{V e^{iA}}{E_f - \epsilon_{i_{\Gamma}}}, \quad (2)$$

where $|\Phi\rangle$ represents the state with a localized electron at the initial site, and $|\Psi^+\rangle$ the state with a localized electron at the final site; E_f is the Fermi energy which will be set to zero, and A is the magnetic vector potential. In principle, the sum is over *all* paths Γ between the initial and final sites (including back-scattering). However, for $V/W \ll 1$, only the shortest (forward scattering) paths need to be included. (For a more detailed discussion and justification on this point, using an analogy with high temperature expansions in the Ising model, see [19,22].) Neglecting back-scattering, we obtain for paths of length t ,

$$\langle i | G(E) | f \rangle = \left(\frac{V}{W} \right)^t J(t), \quad J(t) = \sum_{\Gamma'}^{\text{directed}} \prod_{i_{\Gamma'}} \eta_{i_{\Gamma'}} e^{iA}. \quad (3)$$

The sum is now restricted to directed paths Γ' , and $\eta_i = \text{sign}(\epsilon_i) = \pm 1$. The interference information is captured in the function $J(t)$, while the factor $(V/W)^t$ is the leading contribution to the expected exponential decay of the localized wavefunction.

The transfer matrix approach provides an efficient numerical algorithm for computing $J(t)$. As described in reference [22], this method allows summing over the exponentially large number of paths in polynomial time (typically $\sim t^D$ for D dimensions). The results of extensive analytical and numerical studies (mostly in $D = 2$) based on this method are discussed in reference [19]. Briefly, the probability distribution for $J(t)$ is quite broad. Its *logarithm* is a universal function with a mean is proportional to t , and variance growing as $t^{2\omega}$, with ω depending on the dimension D . Since the mean and variance of the (log-) distribution are independent, *two parameters* are necessary to describe the tunneling probability. High

moments of the distribution are however nonuniversal, and dominated by exceptionally good samples [23].

In discussing the change in the tunneling probability in a magnetic field B , NSS introduced [5] the important concept of the effective ‘cigar’-shaped area through which the field penetrates. Naively, typical directed paths execute a random walk in the transverse direction, so that a path of length t wanders away a distance of the order of $t^{1/2}$. As shown in Fig. 2 the area presented to a magnetic field perpendicular to such paths thus grows as $A_{\perp} \propto t \times t^{1/2} \propto t^{3/2}$, and the MC is expected to be a function of the flux $Bt^{3/2}$. This is indeed the case in the absence of randomness, where the exact response of the sum over directed paths in $D = 2$ [13] initially decreases as B^2t^3 . The above argument does not work in the presence of randomness, where typical paths have super-diffusive transverse fluctuations that grow as t^{ζ} with $\zeta > 1/2$ [22]. However, the scaling functions *are not* simply modified to depend on $Bt^{1+\zeta}$. In the presence of spin-orbit (SO) scattering, the behavior is qualitatively similar to the pure case: there is a positive MC, initially scaling as B^2t^3 , which saturates at a finite (t independent) value. By contrast, in the absence of SO, the (positive) MC grows unbounded with t . This is because the effect of the magnetic field is a (nonuniversal) increase in the localization length ξ , initially scaling as $B^{1/2}$. The appropriate scaling variable in this case is Bt^2 , although numerically one finds a small pre-asymptotic regime with $Bt^{3/2}$ scaling. There is currently no satisfactory explanation of the crossovers in the absence of SO.

The replica arguments [19] suggest that the same asymptotic behavior for the MC should be observed in $D = 3$, as long as the magnetic field is perpendicular to the hopping direction. However, it is also possible to consider fields parallel to the hop. The transverse area presented to the magnetic field by typical diffusive paths (see Fig. 2) now grows as $A_{\parallel} \propto t^{1/2} \times t^{1/2}$, suggesting $B_{\parallel}t$ as the appropriate scaling argument. This simple argument was first presented in ref. [26], along with preliminary numerical support. The anisotropic field dependence was verified recently by Lin and Nori [27] in the IPA approach. In the next section we present detailed numerical results pertaining to the anisotropy of MC in $D = 3$.

III. NUMERICAL RESULTS FOR A SINGLE HOP

As the distribution of the tunneling amplitude $J(t)$ in eq.(3) is broad, care in averaging is quite important. We typically averaged the logarithm of the transition probability (log-conductance) over 2000 realizations of randomness. The transfer matrix method allows us to examine systems of size $t = 600$ in the wedge geometry. Furthermore, after studying the dependence of the computed amplitudes on the lateral dimension, we also used a bar geometry with dimensions $1500 \times 200 \times 200$. This is reasonable if the important paths have transverse fluctuations smaller than 200, which was found to be the case. As discussed before, our main focus is on the different responses for fields parallel and perpendicular to the hop direction. We discuss separately the MC with and without SO scattering. The results in the presence of SO are easily interpreted and offer no fundamental surprises. However, most of our numerical results in the absence of SO pertain to a pre-asymptotic regime for which we have no satisfactory theoretical understanding, but which are most probably of experimental importance.

A. MC without Spin-Orbit Scattering

Fig. 3 shows the MC and its fluctuations for a magnetic field *parallel* to the hopping direction. For the largest values of B , it is clear that $\ln(|J(t, B)|/|J(t, 0)|)^2$ grows linearly with the length t of the hop. This is indicative of an exponential correction to the conductance due to an increased localization length in the magnetic field. It is only after about $t = 400$ that reasonable linearity is achieved, so rather large systems must be examined to study the true asymptotic limit. A similar positive MC (and increased localization length) behavior is also observed for the perpendicular field orientation. Concurrently, there is a reduction in the magnitude of the fluctuations in the tunneling probability (inset Fig. 3), and there appear to be strong correlations between changes in the average of the log-conductance and its fluctuations. This is also the case in $D = 2$, where a replica argument suggests that

these two quantities (indeed the whole probability distribution) are governed by a single parameter [19,22].

Most of the data in Fig. 3 pertains to a pre-asymptotic regime, before the change in localization length becomes apparent. Since the length of the hop in most experiments is only of the order of 20 to 50 ξ , it is useful to explore this regime carefully. In Fig. 4 we present an attempt to collapse the numerical data in this regime for different values of B and t . The collapse for the parallel field orientation is demonstrated in Fig. 4a; the maximum hopping length in this graph is $t = 600$, while fields go up to 0.1 flux quanta per plaquette; all in the pre-asymptotic regime. The choice of the scaling variable $B_{\parallel}t$, is consistent with the flux through a section of the NSS ‘cigar’ perpendicular to the hop direction ($A_{\parallel} \propto \sqrt{t} \times \sqrt{t}$). Two regimes are apparent in Fig. 4a: (i) for the lowest fields ($5 \times 10^{-5} \phi_o$ per plaquette) and sizes ($t = 10 - 100$) there is a linear increase with the variable Bt . (ii) For intermediate fields and hop sizes, when approximately one flux quantum penetrates the NSS ‘cigar,’ there is a non-trivial apparent exponent. The behavior in these regimes is summarized by

$$\left\langle \ln \frac{|J(t, B_{\parallel})|^2}{|J(t, 0)|} \right\rangle = \begin{cases} 1.5 B_{\parallel} t & \text{for } B_{\parallel} t \leq 1 \\ (a_1 B_{\parallel} t)^{\alpha_1} & \text{for } B_{\parallel} t > 1 \end{cases}, \quad (4)$$

where $\alpha_1 = 0.38 \pm 0.02$.

The corresponding collapse for fields in the perpendicular orientation is presented in Fig. 4b. In this case the appropriate scaling variable is $Bt^{3/2}$, again consistent with the flux through the NSS ‘cigar.’ Once more, two different regimes are identified, with

$$\left\langle \ln \frac{|J(t, B_{\perp})|^2}{|J(t, 0)|} \right\rangle = \begin{cases} 0.6 B_{\perp} t^{3/2} & \text{for } B_{\perp} t^{3/2} \leq 1 \\ (b_1 B_{\perp} t^{3/2})^{\alpha_2} & \text{for } B_{\perp} t^{3/2} > 1 \end{cases}, \quad (5)$$

and $\alpha_2 = 0.25 \pm 0.02$. We again emphasize that the second regime above is still pre-asymptotic. For larger systems ($200 \times 200 \times 1500$) the log-conductance crosses over to a regime where presumably the relevant scaling variable is Bt^2 [19]. The latter scaling suggests that the magnetic length is the relevant length scale [24]. We were not able to clearly access this regime as cumbersomely large systems must be simulated.

It is interesting to compute, on the basis of the above results, the anisotropy in conductance of a single critical resistor. We shall define an anisotropy parameter,

$$\beta(B, t) = \frac{\langle \ln |J(t, B_{\perp} = B)|^2 - \ln |J(t, 0)|^2 \rangle}{\langle \ln |J(t, B_{\parallel} = B)|^2 - \ln |J(t, 0)|^2 \rangle},$$

thus making contact with the original experimental definition of ref. [2]. Depending on the strength of the magnetic field, this anisotropy shows different scaling forms: For the smallest fields, such that $Bt^{3/2} < 1$,

$$\beta = \frac{0.6Bt^{3/2}}{1.5Bt} = 0.4t^{1/2}.$$

In this range the anisotropy is field independent, but changes with temperature since $t = \xi(T_0/T)^{1/4}$. There is an intermediate regime where $Bt^{3/2} > 1$ while $Bt < 1$, and

$$\beta \propto B^{\alpha_2-1} t^{1.5\alpha_2-1},$$

which depends on both B and t . Finally, for $Bt > 1$,

$$\beta \propto B^{\alpha_2-\alpha_1} t^{1.5\alpha_2-\alpha_1},$$

which, using the numerically estimated values, is approximately independent of t , and has a weak field dependence as $\beta \propto 1/B^{0.13}$. Thus anisotropy is reduced when the field increases as shown in Fig. 5. Qualitatively similar behavior is observed in *InO* samples for sufficiently high fields in ref. [25].

B. MC with Spin-Orbit Scattering

When spin-orbit active impurities (doping with heavy elements) are taken into account, the NSS model must be generalized to include scattering of the spins. The tight binding Hamiltonian is now modified to

$$\mathcal{H} = \sum_{i,\sigma} \epsilon_i a_{i,\sigma}^{\dagger} a_{i,\sigma} + \sum_{\langle ij \rangle, \sigma\sigma'} V_{ij,\sigma\sigma'} a_{i,\sigma}^{\dagger} a_{j,\sigma'} \quad , \quad (6)$$

where σ indicates the electron spin. The constant nearest-neighbor hopping elements V in eq.(1) are no longer diagonal in spin space. Instead, each is multiplied by U_{ij} , a randomly

chosen $SU(2)$ matrix which describes the spin rotation due to strong SO scatterers on each bond [16,28]. Eq.(2) for the overlap of wave-functions at the two end-points must now include the initial and final spins, and has the locator expansion

$$\langle i\sigma|G(E)|f\sigma'\rangle = \sum_{\Gamma} \prod_{i_{\Gamma}} \frac{Ve^{iAU}}{E_f - \epsilon_{i_{\Gamma}}}. \quad (7)$$

Each bond along the path contributes a random spin rotation U , and a phase factor from the magnetic vector potential A , resulting in

$$\begin{aligned} \mathcal{A} &= \langle i\sigma|G(0)|f\sigma'\rangle = W(V/W)^t J(t); \\ \text{with} \quad J(t) &= \sum_{\Gamma'} \prod_{i_{\Gamma'}} \eta_i e^{iAU}. \end{aligned} \quad (8)$$

After averaging over the initial spin, and summing over the final spin, the tunneling probability is

$$\begin{aligned} T &= \frac{1}{2} \text{tr}(\mathcal{A}^\dagger \mathcal{A}) = W^2 (V/W)^{2t} I(t); \\ \text{with} \quad I(t) &= \frac{1}{2} \text{tr}(J^\dagger J). \end{aligned} \quad (9)$$

For a three dimensional lattice we studied numerically the statistical properties of $I(t)$. Using a transfer matrix we evolve paths of length $t = 600$ in the wedge geometry, averaging over 2000 realizations of randomness. As in the previous section, we also used the bar geometry to compute $I(t)$ for systems of size $200 \times 200 \times 1500$. We checked the bar-geometry results for crossover effects (because of the smaller lateral sizes) and confirmed that their behavior is effectively three dimensional. The numerical results are shown in Fig. 6, and have the same qualitative features as in two dimensions: Unlike in the absence of SO, there is no linear increase of $\Delta \ln I_{so}(B, t)$ with system size t , and the MC saturates to a field dependent value for sufficiently long hops. The scale of fluctuations in (the logarithm of) $I(t)$ is not significantly modified by the B field. As in $D = 2$, turning on the SO scattering from zero, thus switching from an orthogonal to a symplectic Hamiltonian, is accompanied by an increase in the zero field conductance, and a concomitant reduction in conductance fluctuations.

Fig. 7 demonstrates the collapse of the MC data for fields both parallel and perpendicular to the hopping direction. For fields parallel to the hopping direction the appropriate scaling parameter is again $B_{\parallel}t$, corresponding to the flux through the area $A_{\parallel} \propto (\sqrt{t})^2$. The scaling function has the form

$$\langle \ln I(t, B_{\parallel}) - \ln I(t, 0) \rangle = \begin{cases} 0.4B_{\parallel}^2 t^2 & \text{if } B_{\parallel}t < 1 \\ C \approx 0.2 & \text{if } B_{\parallel}t > 1 \end{cases}. \quad (10)$$

For fields in the perpendicular orientation, the appropriate area is $A_{\perp} \propto t^{3/2}$ (see Fig. 2), leading to a scaling function

$$\langle \ln I(t, B_{\perp}) - \ln I(t, 0) \rangle = \begin{cases} 0.1B_{\perp}^2 t^3 & \text{if } B_{\perp}t^{3/2} < 1 \\ C \approx 0.2 & \text{if } B_{\perp}t^{3/2} > 1 \end{cases}. \quad (11)$$

The saturation value, when one flux quantum threads the appropriate area, is roughly the same in the two cases.

The anisotropy parameter in the presence of SO is

$$\beta = \begin{cases} 0.25t & \text{if } Bt^{3/2} < 1 \\ 1 & \text{if } Bt > 1 \end{cases},$$

with a small crossover region between $Bt^{3/2} \sim 1$ and $Bt \sim 1$. We thus obtain a hopping size dependent anisotropy (which might show up as a temperature dependent anisotropy) for low fields. For higher fields, anisotropy in the presence of SO scattering disappears as the field is increased beyond a flux quantum through the smaller of the typical areas found above. In order to properly compare with experiments, one must average over different magnetic fields orientations as discussed in the next section.

The MC in the presence of SO can be explained by a replica analysis. After averaging over the impurity potential $\epsilon_i = \pm W$, the moment $\langle I(B, t)^n \rangle$, is obtained as a sum over n paired paths. The pairings either involve paths taken from J and J^{\dagger} ; the contributions from the magnetic vector potential cancel for such ‘neutral’ pairs, which do not contribute to the MC. It is also possible to construct pairs with both paths taken from either J or J^{\dagger} ; such ‘charged’ paths are responsible for magnetic response. An interesting feature of averaging over strong SO scatterers (the matrices U in eq.(8)) is that the charged and neutral paths

become completely decoupled and can be treated independently [19]. Thus the MC with SO is (rather fortuitously) calculated exactly by IPA: there is no change in the localization length, and only a constant increase in the tunneling amplitude. Recently Lin and Nori [27] computed the field dependencies in a scheme that is equivalent to IPA in two and three dimensions. (The equivalence to IPA can be readily recognized from the equality of the moments of the ‘conductance’ to those of a Gaussian obtained in ref. [9].) In the small field limit Lin and Nori confirm exactly the scaling variables derived by us [26] here, for the two field orientations. Another notable feature of the data is the B^2 dependence for small fields, as expected in the IPA approach [9].

IV. AVERAGING OVER MANY HOPS

So far we focused on the response of a single hop to a magnetic field. However, the percolation arguments [10] [11] for the Miller-Abrahams network leads to the conclusion that critical resistors dominate only over a correlation length ℓ . Starting from the properties of a percolation cluster near the threshold it is concluded [21] that a single hop is responsible for the overall conductivity only for length scales up to

$$\ell \sim \xi \left(\frac{T_0}{T} \right)^{\frac{\nu+1}{D+1}}, \quad (12)$$

where ν is the exponent for the divergence of the correlation length close to the percolation threshold. The macroscopic system is then built by superposing many blocks of length ℓ . Therefore, in general, many critical hops, in general, contribute to the conductivity of a large sample. In eq.(12) the variable T_0/T can be regarded as a measure of disorder strength; it increases when the density of states at the Fermi level, or the localization length, decreases. As disorder increases, the volume dominated by the critical NSS resistor gets larger.

For samples of size $L \gg \ell$, many hops contribute to the conductivity, and the overall MC must be calculated from their *average* response. Using the experimentally reported [2] data, we can estimate ℓ : For samples of thickness $d = 100\text{\AA}$ and hopping length $t \approx 3 - 4d$,

one obtains $\ell \approx 1000\text{\AA}$. Although this length is large compared to the sample thickness, it is still very small in comparison to the sample planar dimensions (10×6 mm for the experiments in reference [2]). Many hops thus influence the conductance of these samples, each with a presumably different orientation with respect to the magnetic field. In the following paragraphs we shall perform an average over the directions of the NSS ‘cigar’-shaped region with respect to the magnetic field. We shall assume that the electric field is sufficiently weak so that the relative orientations of the hops are still randomly distributed in space [20,29]. We expect that for thick samples (as compared to the hopping length t) the averaging over all possible directions of the hop removes the anisotropy in MC, as seen in experiments. On the other hand, for thin samples such that $d \leq t$, the restricted averaging over effectively two-dimensional hops should lead to significant field anisotropy. Such thickness dependent anisotropy is indeed observed in the experiments of Faran and Ovadyahu [2], and those of Orlov and Savchenkov [1,7].

We shall assume that the appropriate ‘cigar’ shaped region for calculating magnetic interference phenomena is an ellipsoid of revolution as depicted in Fig. 8. The major and minor axes of the ellipsoid are denoted by b and a respectively. Following NSS, $2b \equiv t$ is the length of the dominant hop, while $a = \sqrt{t\xi}$ is a typical diffusive distance in the transverse direction. Consider a magnetic field B at an angle θ_t with respect to the major axis. We take the relevant magnetic flux to be that which penetrates the projection of the ellipsoid onto a plane perpendicular to the B field, as indicated in Fig. 8. This projection is an ellipse of minor axis a , and with a major axis of length $c = \sqrt{a^2 \cos^2 \theta_t + b^2 \sin^2 \theta_t}$. In previous sections we demonstrated that in the weaker field regimes $\Delta \ln |J(B, t)|^2 \propto \langle |\Phi|^\gamma \rangle$, where Φ is the appropriate flux. In the presence of SO, $\gamma = 2$ as justified by IPA, while $\gamma = 1$ in the absence of SO from the numerical results. In the following, we shall focus on $\gamma = 2$ with SO, which has a better justification, and for which it is easier to compute the average,

$$\begin{aligned} \langle \Phi^2 \rangle &= \langle (\pi a c B)^2 \rangle \\ &= \pi^2 B^2 a^2 \left[b^2 - (b^2 - a^2) \langle \cos^2 \theta_t \rangle \right]. \end{aligned} \quad (13)$$

In performing the average over hop orientations θ_t , we distinguish between the following regimes:

(i) The behavior of samples of thickness $d \gg t$ is effectively three dimensional. All orientations θ_t are equally likely (in low voltage bias), and $\langle \cos^2 \theta_t \rangle = 1/3$. The averaged response is isotropic and depends upon

$$\langle \Phi^2 \rangle = \frac{B^2 \pi^2 a^2}{3} (2b^2 + a^2). \quad (14)$$

The characteristic B^2 dependence is a signature of the IPA, and is also observed experimentally for small fields. In fact, the flux through a typical interference region in ref. [2] is of the order of $0.5hc/e$ which corresponds to the regime $Bt^{3/2} < 1$.

(ii) For $a \ll d \simeq t$, the range of orientations of the cigar is limited by the finite thickness, leading to MC anisotropy. Consider a magnetic field at an angle α with respect to the plane of the sample. We shall indicate the orientation of the major axis of the ellipsoid by a polar angle θ (with respect to the normal to the sample), and an azimuthal angle ϕ . Because of the finite thickness, the range of $\cos \theta$ is limited to the interval $[-d/2b, +d/2b]$, and allowed angles in this range are weighted by

$$p(\cos \theta) = \begin{cases} 2b/d - 4b^2 |\cos \theta|/d^2 & \text{if } |\cos \theta| < d/2b \\ 0 & \text{if } |\cos \theta| > d/2b \end{cases}. \quad (15)$$

The relative angle between the field and the major axis of the ellipsoid is obtained from

$$\cos \theta_t = \cos \alpha \sin \theta \cos \phi + \sin \alpha \cos \theta. \quad (16)$$

Since all azimuthal angles are possible $\langle \cos \phi \rangle = 0$, while $\langle \cos^2 \phi \rangle = 1/2$; and from eq.(15) $\langle \cos^2 \theta \rangle = d^2/8b^2$. Thus, we finally arrive at

$$\langle \cos^2 \theta_t \rangle = \frac{d^2}{8b^2} + \frac{\cos^2 \alpha}{2} \left(1 - \frac{3d^2}{16b^2} \right), \quad (17)$$

which describes the MC anisotropy, when substituted in eq.(13).

(iii) Another limit that is easily accessible is for $d \simeq a$. Now all the ellipsoids lie in the plane, and $\cos \theta = 0$, leading to $\langle \cos^2 \theta_t \rangle = \cos^2 \alpha/2$. From eq.(13) we then obtain

$$\langle \Phi^2 \rangle = \frac{B^2 \pi^2 a^2}{2} \left[2b^2 - (b^2 - a^2) \cos^2 \alpha \right]. \quad (18)$$

This particular limit is plotted in Fig. 9, and can be compared to experimental data for the angular dependence of MC (at fixed temperature and field strength). The parameters $a = \sqrt{t\xi}$ and $2b = t$ in this figure are chosen to correspond with those reported in ref. [2]. The general form of the curve agrees qualitatively with the experimental data. Another pertinent comment concerns the experimental data of Laiko et al [7]: they compare results for fields parallel and perpendicular to the current direction (while the field is in the plane of the sample). On averaging over hop directions, the MC for these configurations should be identical, in agreement with experiments, except for very disordered samples where ℓ is so large that averaging is not appropriate.

(iv) Finally for $d < a$, the NSS cigar is flattened into a pancake and is no longer ellipsoidal. The behavior is generally two dimensional, with $\Phi = \pi ab \times B \sin \alpha$. This formula breaks down only at very small angles such that $\alpha \leq d/b$, for which $\langle \Phi^2 \rangle \approx (B\pi da)^2/2$.

Clearly, the general tendency is that as temperature is reduced (hence $2b = t$ is increased), the ratio d/t gets smaller. As indicated by the above sequence, this leads to more and more pronounced effects in the MC anisotropy. This is indeed consistent with the experimental observations. In principle, the temperature dependence of this increase could be measured experimentally and compared to the above theoretical formulas.

V. DISCUSSION

In this paper we studied the NSS model for quantum interference effects of a tunneling electron in $D = 3$. The three dimensional geometry allows us to consider the relative orientations of the hop and the magnetic field. The effect of both spin-orbit active and inactive impurities were taken into account. The results indicate that, in the absence of SO impurities, there is positive MC due to an increase in the localization length for fields both parallel and perpendicular to the hop direction. Furthermore, the MC data for different

fields collapses onto universal curves using the scaling variables $B_{\perp}t^{3/2}$, and $B_{\parallel}t$ for the two orientations. This implies that, at least in the low field regime, crossover effects are controlled by the flux penetrating an NSS ‘cigar’ whose transverse size grows diffusively (as \sqrt{t}).

In the presence of SO impurities, the numerical results again indicate a positive MC, but as in two dimensions, no change in the localization length is observed. No reduction in the fluctuations is obtained in agreement with the replica arguments [19]. The results in this case are the same as those obtained from an independent path approximation. The MC grows initially as B^2 for both parallel and perpendicular orientations as expected. Its anisotropy disappears for large enough fields as the MC saturates to roughly the same constant in both directions. This could be checked experimentally in the thin film limit ($d < t$) for samples doped with heavy elements.

The most spectacular manifestation of these results is the possibility of observing *bulk MC anisotropy*, when the sample is small enough (or the characteristic length $\ell = \xi(T_0/T)^{(\nu+1)/(D+1)}$ is large enough) that only a single hop (or just a few) dominates the macroscopic conductance. The sample will then exhibit a ‘finger-print’ in its MC anisotropy, and the random orientation of the critical hop can be determined by bulk anisotropy measurements. (It is possible that this phenomenon explains why the experiments of Laiko et al [7] go from isotropic to anisotropic behavior as disorder is increased [30].) Large values for ℓ may be achieved by either choosing samples with lower density of states at the Fermi level, or larger t/ξ . Other manifestations of the *disorder length scale* (including bulk MC anisotropy) may occur under strong voltage bias [29], if the electric field reorients the critical hops; constraining the average over hop orientations to within a cone.

However, the conductance of most samples with $L \gg \ell$ is governed by many hops. Our estimate of ℓ based on published experimental data [2] indicates that it is much smaller than typical sample planar dimensions. Thus, averaging over many hop orientations is inevitable, washing out the predicted anisotropy finger-print of a single hop. Nevertheless, anisotropic

behavior is still expected for sufficiently thin samples (or at low temperatures). This is because when the length of the cigar becomes comparable or larger than sample thickness ($t > d$), the hops are forced to lie mostly parallel to the sample plane. This restriction on hop orientations then leads to an MC anisotropy that becomes more and more pronounced upon lowering temperature. Appearance of such anisotropy in thin films has already been observed in insulating *InO* samples [25,8]. In principle, the variations of anisotropy with temperature can be measured accurately and compared to the formulas derived in the previous section. Measurements of anisotropy can thus provide an additional experimental tool for tests of quantum interference models.

ACKNOWLEDGMENTS

We have benefited from discussions with R. F. Angulo and M. Araujo. MK is supported by the NSF through grant number DMR-93-03667. EM thanks INTEVEP S.A. for permission to publish this paper. This work was supported by the MIT-INTEVEP Collaborative Research Agreement.

REFERENCES

- [1] A. O. Orlov and A. K. Savchenko, Pis'ma Zh. Eksp. Teor. Fiz. **44**, 34 (1986) [JETP Lett. **44**, 41 (1986)].
- [2] O. Faran and Z. Ovadyahu, Phys. Rev. B **38**, 5457 (1988).
- [3] F. P. Milliken and Z. Ovadyahu, Phys. Rev. Lett. **65**, 911 (1990).
- [4] Y. Zhang, P. Dai, and M. P. Sarachik, Phys. Rev. B **45**, 9473 (1992).
- [5] V. L. Nguyen, B. Z. Spivak, and B. I. Shklovskii, Pis'ma Zh. Eksp. Teor. Fiz. **41**, 35 (1985) [JETP Lett. **41**, 42 (1985)]; Zh. Eksp. Teor. Fiz. **89**, 11 (1985) [Sov. Phys. JETP **62**, 1021 (1985)].
- [6] N. F. Mott, J. Non-Cryst. Solids **1**, 1 (1968).
- [7] E.I. Laiko, A. O. Orlov, A.K. Savchenkov, E. A. Il'ichev and E. A. Poltoratskii Zh. Eksp. Teor. Fiz. **93**, 2204 (1987) [Sov. Phys.-JETP **66**, 1258 (1987)]; Z. Ovadyahu, J. Phys. C **19**, 5187 (1986); Ya. B. Poyarkov, V. Ya Kontarev, I. P. Krylov, and Yu. V. Sharvin, Pis'ma Zh. Eksp. Teor. Fiz. **44**, 291 (1986) [JETP **44**, 372 (1986)].
- [8] M. Eto, Physica B **194**, 1113 (1994).
- [9] U. Sivan, O. Entin-Wohlman, and Y. Imry, Phys. Rev. Lett. **60**, 1566 (1988); Phys. Rev. B **40**, 8342 (1989).
- [10] V. Ambegaokar, B. I. Halperin, and J. S. Langer, Phys. Rev. B **4**, 2612 (1971).
- [11] B. I. Shklovskii and A. L. Efros, Zh. Eksp. Theor. Fiz. **60**, 867 (1971); Sov. Phys. JETP **33**, 468 (1971).
- [12] Y. Shapir and X. R. Wang, Europhys. Lett. **4**, 1165 (1987).
- [13] E. Medina, M. Kardar, Y. Shapir, and X. R. Wang, Phys. Rev. Lett. **62**, 941 (1989); **64**, 1816 (1990).

- [14] J. L. Pichard, M. Sanquer, K. Slevin, and P. Debray, Phys. Rev. Lett. **65**, 1812 (1991);
Y. Avishai, J. L. Pichard, and K. A. Muttalib, J. Phys. I. **3**, 2342 (1993); and see also,
I. V. Lerner and Y. Imry, preprint (1994).
- [15] Y. Shapir and Z. Ovadyahu, Phys. Rev. B **40**, 12441 (1989).
- [16] Y. Meir, N. S. Wingreen, O. Entin-Wohlman, and B. L. Altshuler, Phys. Rev. Lett. **66**,
1517 (1991).
- [17] E. Medina and M. Kardar, Phys. Rev. Lett. **66**, 3187 (1991).
- [18] P. W. Anderson, Phys. Rev. **109**, 1492 (1958).
- [19] E. Medina and M. Kardar, Phys. Rev. B **46**, 9984 (1992).
- [20] A. Miller and E. Abrahams, Phys. Rev. B **120**, 745 (1960).
- [21] B. I. Shklovskii and A. L. Efros, *Electronic Properties of Doped Semiconductors*
(Springer-Verlag, Berlin, 1984).
- [22] M. Kardar, *Lectures on Directed Paths in Random Media*, Les Houches Summer School
on Fluctuating Geometries in Statistical Mechanics and Field Theory, August 1994 (to
be published; see cond-mat/9411022).
- [23] E. Medina and M. Kardar, J. Stat. Phys. **71**, 967 (1993).
- [24] For other numerical results see, B. Spivak, H. L. Zhao, and S. Feng, JETP Lett. **59**,
629 (1994).
- [25] Z. Ovadyahu, S. Moehlecke, and Y. Imry, Surf. Sci. **113** 544, (1982); T. Ohyama, M.
Okamoto, and E. Otsuka, J. Phys. Soc. Jap. **52**, 3571 (1983).
- [26] E. Medina, M. Kardar, and R. Rangel, Bull. Amer. Phys. Soc. **39**, 348 (1994).
- [27] Y.-L. Lin and F. Nori, preprint (1995).
- [28] N. Zannon and J. L. Pichard, J. Phys. (France) **49**, 907 (1988).

- [29] V. L. Nguyen and B. I. Shklovskii, Sol. State Comm. **38**, 99 (1981).
- [30] Notice that in those experiments one cannot distinguish between results (for fields parallel to the plane) either in the direction of the current or perpendicular to it unless disorder is large enough (Fig.(6) of Laiko et al).

FIGURES

FIG. 1. The NSS model on a three dimensional diagonal lattice. Impurities are located on the sites.

FIG. 2. The figure depicts how effective areas that arise from scaling can be derived from random walk arguments.

FIG. 3. Log-conductance as a function of system size t for fields parallel to the hop direction. The change in the slope with the field indicates an exponential correction to the conductance (change in the localization length). A straight line is drawn as a guide to the eye. The inset shows a reduction of fluctuations with the field. The power law dependence on the hopping length is also indicated.

FIG. 4. The figure shows the collapse of the log-conductance data with the appropriate scaling variables (a) Bt in the case the field is parallel to the hop and (b) $Bt^{3/2}$ for fields perpendicular to the hop direction. The scaling variable tells about the relevant area threaded by the field.

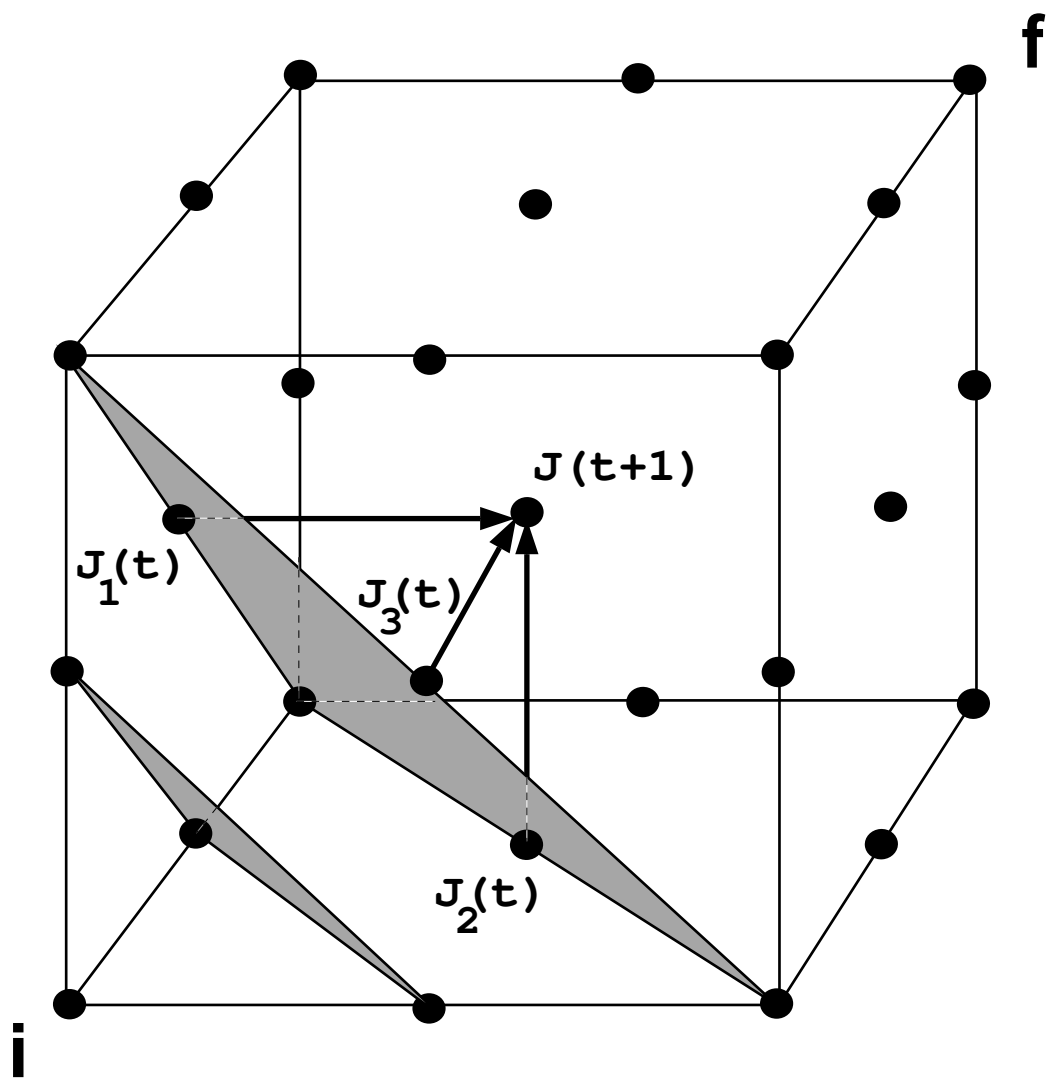
FIG. 5. Field dependencies for parallel and perpendicular field directions when $Bt^{3/2} > 1$ and for a single critical resistor.

FIG. 6. Magnetoconductance in the presence of spin-orbit scattering. The relevant log-conductance is no longer linear in t for large hopping lengths, indicative of no changes in the localization length due to the field.

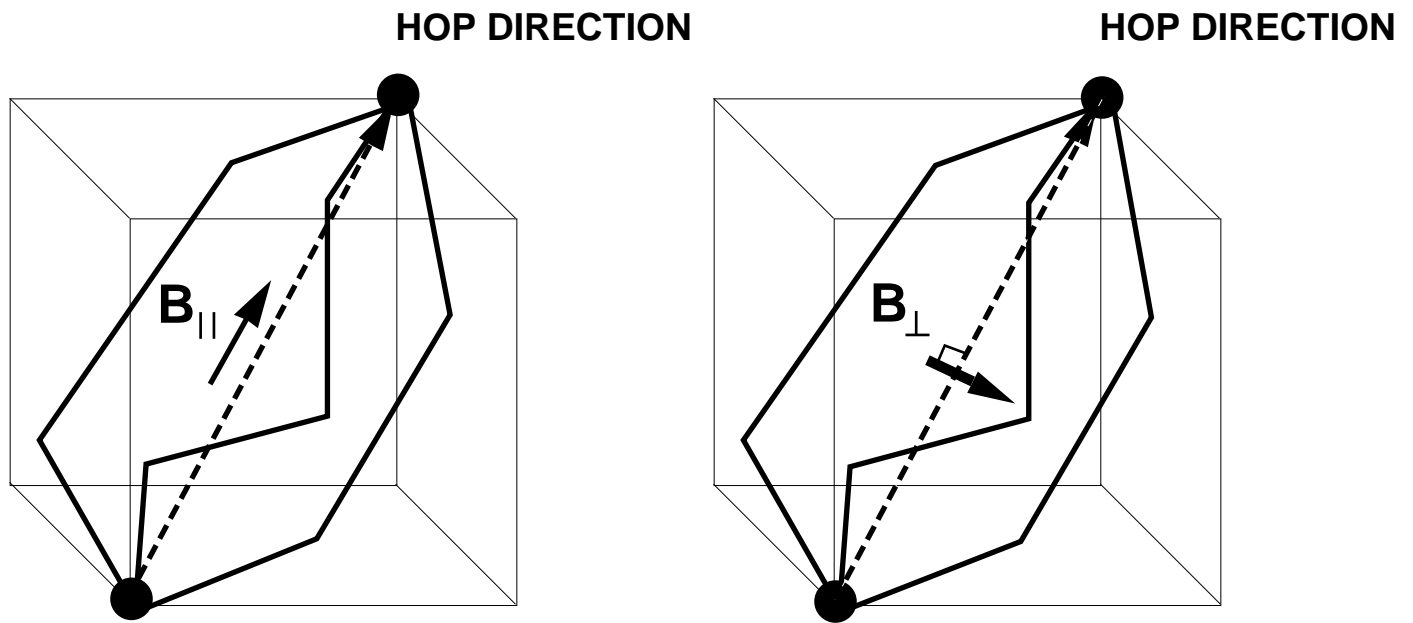
FIG. 7. Collapse of the MC data in the presence of SO scattering. The MC is governed by the areas a) $(\xi^{1/2}t^{1/2})^2$ for fields parallel to a single critical hop and b) $\xi^{1/2}t^{3/2}$ for fields perpendicular to the hop direction.

FIG. 8. Angle convention used to perform averages over critical hop directions. The magnetic field is along the z axis making an angle θ_t with the principal axis of the ellipsoid containing dominant paths. The relevant magnetic flux penetrates through the largest cross section of the ellipsoid perpendicular to the magnetic field i.e. an ellipse of minor axis a and major axis c .

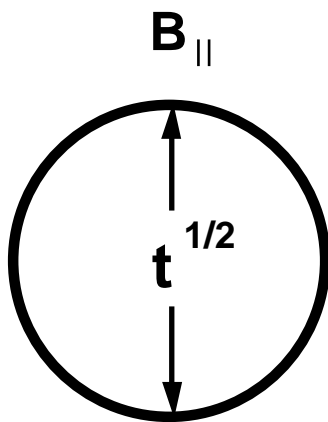
FIG. 9. Theoretical curve computed from eq.(18). The experimental data correponds to $\xi = 85\text{\AA}$, $t = 280\text{\AA}$ and sample thickness $d = 250\text{\AA}$. Notice how the curve fall towards $\alpha = 0$ (parallel to sample), closely resembling the experimental data of reference [2].



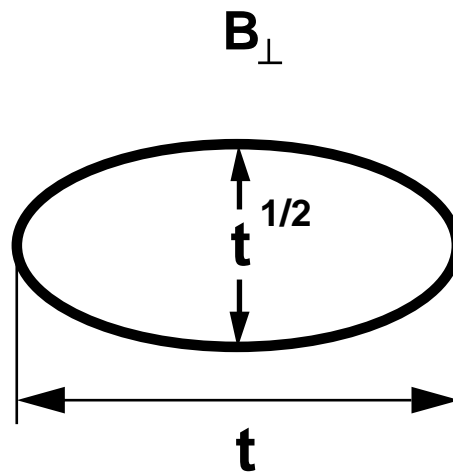
Coherent hop in the Miller-Abrahams network



Effective areas threaded by field



$$A = C t$$



$$A = C t^{3/2}$$

